american physiological society

JNP JOURNAL OF NEUROPHYSIOLOGY

J Neurophysiol 130: 1067–1080, 2023.
First published September 20, 2023; doi:10.1152/jn.00108.2023

RESEARCH ARTICLE

Computational Neuroscience

A personalized cortical atlas for functional regions of interest

M. Fiona Molloy[1,2] and David E. Osher[1]

[1]*Department of Psychology, The Ohio State University, Columbus, Ohio, United States and* [2]*Department of Psychiatry, University of Michigan, Ann Arbor, Michigan, United States*

Abstract

Advances in functional MRI (fMRI) allow mapping an individual's brain function in vivo. Task fMRI can localize domain-specific regions of cognitive processing or functional regions of interest (fROIs) within an individual. Moreover, data from resting state (no task) fMRI can be used to define an individual's connectome, which can characterize that individual's functional organization via connectivity-based parcellations. However, can connectivity-based parcellations alone predict an individual's fROIs? Here, we describe an approach to compute individualized rs-fROIs (i.e., regions that correspond to given fROI constructed using only resting state data) for motor control, working memory, high-level vision, and language comprehension. The rs-fROIs were computed and validated using a large sample of young adults (n = 1,018) with resting state and task fMRI from the Human Connectome Project. First, resting state parcellations were defined across a sequence of resolutions from broadscale to fine-grained networks in a training group of 500 individuals. Second, 21 rs-fROIs were defined from the training group by identifying the rs network that most closely matched task-defined fROIs across all individuals. Third, the selectivity of rs-fROIs was investigated in a training set of the remaining 518 individuals. All computed rs-fROIs were indeed selective for their preferred category. Critically, the rs-fROIs had higher selectivity than probabilistic atlas parcels for nearly all fROIs. In conclusion, we present a potential approach to define selective fROIs on an individual-level circumventing the need for multiple task-based localizers.

NEW & NOTEWORTHY We compute individualized resting state parcels that identify an individual's own functional regions of interest (fROIs) for high-level vision, language comprehension, motor control, and working memory, using only their functional connectome. This approach demonstrates a rapid and powerful alternative for finding a large set of fROIs in an individual, using only their unique connectivity pattern, which does not require the costly acquisition of multiple fMRI localizer tasks.

fMRI; functional connectivity; functional regions of interest; individual differences; parcellation

A PERSONALIZED CORTICAL ATLAS FOR FUNCTIONAL REGIONS OF INTEREST

One of the oldest endeavors in neuroscience concerns mapping the human brain. Early brain mapping approaches delineated regions based on the cytoarchitecture in postmortem brains (1). Advances in neuroimaging, specifically MRI, allowed for the development of atlases in vivo [2; for review, see Dickie et al. (3)]. In both cases, regions of the brain are grouped based on structural similarities, such as cell types, anatomical features, or landmarks. More recently, parcellations have been developed using intrinsic functional connectivity measured by resting state fMRI [for review, see Eickhoff et al. (4)], which capitalize on systematic cofluctuations in brain regions at rest (i.e., without a task). Atlases have practical advances, such as providing a common framework across different studies and populations and reducing high-dimensional data. Furthermore, a major goal in mapping the brain is to expand our theoretical understanding of how the brain operates and supports cognition. Accordingly, atlases should correspond to brain organization and/or function.

Functional connectivity (frequently characterized as a connectome or full pairwise matrices containing the cofluctuations of brain units) is ideal for studying the functional organization of the brain. Analyses of connectomes have revealed robust resting state networks across the lifespan (5) and within individuals (6) characterizing the macroscale organization of the human brain. Group-level resting state networks are associated with different cognitive processes and behavioral domains (7) and can be used alongside task data to

Correspondence: M. Fiona Molloy (mfionamolloy@gmail.com).
Submitted 14 March 2023 / Revised 18 September 2023 / Accepted 18 September 2023

further map networks underlying specific cognitive processes, such as language (8, 9). These resting state patterns vary by individual and relate to individual differences in behavior (10–12). Connectivity differences are also systematically observed in clinical populations (13–15). Importantly, individual resting state patterns are predictive of that individual's neural responses (16–18). These close links to behavior, neural activity, and individual differences make functional connectivity an ideal candidate for parcellating an individual's brain into units corresponding to cognitive processing.

Some cognitive processes, such as the processing of language or faces, are supported by a given region (or regions) of interest specialized for that specific cognitive function (19). These functional regions of interest (fROIs) can be reliably identified on an individual-level using task-based fMRI. Robust subject-level fROIs can be localized in domains including motor control (20, 21), high-level vision (22–25), and language (26–29). For example, face-specialized regions, such as the fusiform face area (30), can be defined by selecting voxels that show a higher response to pictures of faces compared with pictures of objects. Using an individual's fROIs can account for individual differences in the location, size, and shape of these fROIs (31). fROIs also have statistical advantages due to limiting the potential search space and number of tests and practical advances in computational modeling through reducing the number of components (32). Finally, analyses of fROIs present theoretical advantages by allowing researchers to study unique mechanisms within a specific region. For example, evidence has shown that not all scene-processing fROIs have the same functions (33), so if a researcher is interested in scene categorization, as opposed to navigation, focusing on a region specialized for that specific cognitive process, such as the parahippocampal place area (PPA), would be ideal for studying the underlying neural mechanisms. However, to avoid circular analyses (34), these regions have to be identified using an additional task-based localizer scan. Here, we explore the feasibility of using only parcellated functional connectivity to identify key fROIs without a localizer scan across multiple domains of cognitive processing, including motor control, category-specific visual regions, working memory, and language.

Although many individual-level atlases based on functional connectivity have been proposed [for review, see Arslan et al. (35)], the correspondence of resting state parcels to domain-specific modules, or fROIs, is unknown. Broadly, individual-specific resting state parcellations resemble activity during a task, as their boundaries tend to correspond to whole brain task activity (6, 36–38). This correspondence can be quantified using the similarity between the resulting parcellations overall and task activity across the brain, e.g., by assessing the mean variability of z-scores in parcels (37). Critically, individualized parcellations appear to better capture task data than group parcellations (37). Previous approaches consider the entire parcellation and whole brain activity, but can we identify single resting state networks that can approximate key localized functional units? Recent work has demonstrated the potential for defining domain-specific networks by using an individual's functional connectivity to define an individual-specific language network but requires significant user input (either by manually selecting a seed or individual tuning of clustering parameters), limiting the ease of applying this approach to a large number of subjects (39).

Here, we propose an automated method to compute fROIs using only resting state functional connectivity (rs-fROIs) that approximate fROIs for motor control, high-level vision, working memory, and language comprehension. First, networks from resting state parcellations are matched to task data to identify individualized rs-fROIs that have a high overlap with an individual's task-fROIs in the training group of 500 individuals from the Human Connectome Project (40). Second, these rs-fROIs are computed for the test group of 518 individuals using only resting state functional connectivity. Third, we determine if the rs-fROIs in the test set are selective for the expected domain. Fourth, we compare the selectivity of the individualized rs-fROIs to group-level probabilistic atlas parcels. Finally, we determine how the boundaries of the rs-fROIs are preserved across different resolutions of resting state parcellations.

MATERIALS AND METHODS

We used resting state fMRI data from a large cohort from the Human Connectome Project (40) to define parcellations of functional connectivity. From these parcellations, we identified networks that approximate the location of an individual's fROI. These individualized networks, constrained by the search space, are referred to as rs-fROIs, as they can be computed for an individual using only resting state functional connectivity. Figure 1 shows an overview of the parcellation approach, definition of rs-fROIs, and validation of rs-fROIs, described in this paper, which is further elaborated under *Resting State Parcellations*. To summarize, based on dense vertex-to-vertex resting state functional connectivity, we first defined group-level parcellations using k-means clustering for $k = 2$ to 200 total networks. Then, individual-specific parcellations for each k were computed using k-nearest neighbor classification to the group-defined cluster centroids, in an independent set of subjects. To explore the use of resting state parcellations to approximate an individual's fROIs, we next identified rs-fROIs from the above parcellations. In the training stage (Fig. 1*B*), we identified the network, from all parcellations, that had the highest overlap with a given fROI defined from actual task data (i.e., task-fROI), averaging across individuals. The left-hand (LH) fROI is shown as an example. In the test stage (Fig. 1*C*), the rs-fROI is computed from the resting state data (no task data) by determining the personalized parcellation of the network identified in the training stage.

Data

The data were obtained from the Human Connectome Project [HCP; Van Essen et al. (40)]. All individuals ($n = 1{,}113$) were scanned at Washington University in St. Louis (WashU). The study was approved by the WashU institutional review board, and all participants provided written informed consent. The 1,018 HCP subjects (546 females, 472 males) included in this study completed 2 days of scanning using the customized Siemens Skyra 3 T MRI scanner (Siemens, Erlangen, Germany) at WashU. High-resolution (0.7mm^3 isotropic voxels) T1-weighted and T2-weighted structural images were collected for all subjects. An additional 28 individuals rescanned within a year of their first sessions (who were also in the group of individuals in the test stage in Fig. 1) were

included to explore the effect of shorter resting state scans on the resulting rs-fROIs. The resting state runs comprised of gradient-echo planar imaging sequences (TE/TR = 33.1/720 ms, flip angle = 52°, multiband factor = 8, 72 slices, 2 mm isotropic voxels). Two resting state runs were collected each day, for a total of four 15-min runs (1,200 volumes) per individual. On each day, one run was encoded in a right-to-left direction and the other was encoded in a left-to-right direction. Subjects were instructed to keep their eyes open with relaxed fixation on a projected cross on a dark background.

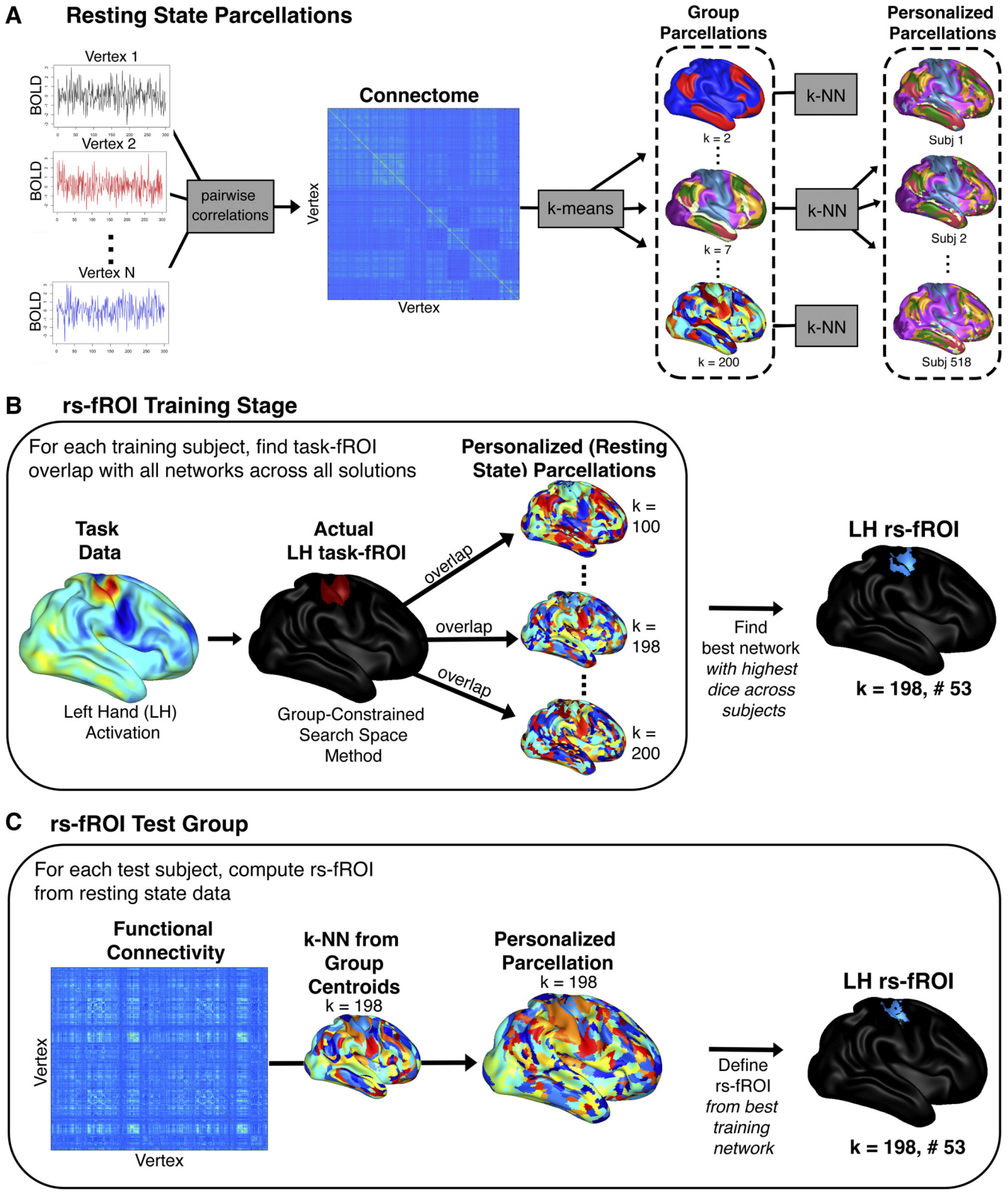

The task data used to determine and validate rs-fROIs also come from the HCP (41). Here, we explore three tasks with key contrasts chosen to localize fROIs in the domains of motor function (e.g., hand – average), high-level vision (e.g., faces – average), working memory (2 back – 0 back), and language comprehension (e.g., story – math). The motor strip mapping task involved blocks of moving left/right hands and feet and tongue following a visual cue. The category representations (tools, places, faces, and bodies) were embedded in a 2-back and 0-back working memory task. Finally, the task chosen to localize language comprehension included blocks where participants either: listened to a short story and answered comprehension questions (story condition) or listened to and solved addition and subtraction problems (math condition). Further task parameters and group-level results are detailed in the study by Barch et al. (40). fMRI acquisition parameters were identical to those used in the resting state scans, apart from the duration of the tasks. Two runs were collected per task.

Preprocessing

The resting state data were preprocessed following the HCP minimal preprocessing pipeline [Glasser et al. (42)]. In brief, preprocessing included artifact correction (gradient nonlinearity and echo-planar imaging distortion correction), motion correction, automated independent component analysis temporal denoising using ICA-FIX (43), and registration to MNI152 template space. The volume time series were then mapped to the standard CIFTI grayordinate space (91,282 vertices). Individual connectomes were defined as the Fisher-transformed Pearson correlation between the time series (concatenated across all 4 runs) of each cortical grayordinate. To define the group-level connectome, we randomly sampled 500 subjects without replacement from the 1,018 HCP subjects with four 15-min runs of resting state data (training group). The remaining 518 subjects comprise the test group. For the 28 individuals in the retest group, four individual connectomes were defined for each individual, for each of the four runs from the retest session (e.g., connectomes were defined from a single 15-min resting state run, as opposed to concatenated 60-min of resting state data). For preprocessing of the task data, we again used the HCP pipeline [(41, 42) using FEAT from FSL (FMRIB Software Library)] and selected a 12-mm smoothing kernel to ensure maximal overlap across the group.

Resting State Parcellations

Group-level parcellations were calculated from the full connectome using a *k*-means algorithm (44, 45) along a sequence of *k* (number of clusters) from $k = 2$ to 200, with five replicates and a cosine distance metric (1 minus the cosine of the angle between points). Individual-level parcellations were defined using *k*-nearest neighbor (*k*-NN) classification.

The *k*-centroids were specified according to the centroids from the above group-level parcellations. Vertices were assigned to a network based on which the network maximized the similarity (cosine) between the individual vertex's connectivity profile in that individual and a given network's centroid connectivity profile. Individual parcellations were then mildly denoised via morphological opening (46), i.e., one step of dilation followed by one step of erosion, which preserves shape while filling in single-vertex holes.

rs-fROI Training Stage

Here, we focus on 21 putative fROIs: five motor regions (right hand, left hand, right foot, left foot, and tongue), six language regions [Fedorenko et al. (26)], one set of distributed regions corresponding to working memory, and nine high-level visual regions (23). The visual regions included two tool regions, lateral occipital (*tool 1*: LO) and posterior fusiform sulcus (*tool 2*: PFS); three place regions, parahippocampal place area (*place 1*: PPA), retrosplenial cortex (*place 2*: RSC), and transverse occipital sulcus (*place 3*: TOS); three face regions, fusiform face area (*face 1*: FFA), occipital face area (*face 2*: OFA), and superior temporal sulcus (*face 3*: STS), and one body region, extrastriate body area (EBA). Task fROIs were defined on an individual level based on group-constrained subject-specific (GSS) fROIs (26). The GSS method consists of two steps: *1*) mask individual subject data with a domain-specific search space and *2*) define individual task activation for a given contrast.

A search space is the region of the cortex where a putative fROI is most likely to be in most individuals. The search spaces for high-level vision and language comprehension are defined from previous literature (23, 26), which constructed search spaces for these domains in independent localization datasets. However, search spaces have not been explicitly created for motor control and working memory, so for the motor and working memory fROIs, search spaces were defined from the HCP data as areas with group overlap above 60%. Group overlap was defined as the percentage of individuals with significant activation ($P < 0.05$) at a given vertex. Discontinuous components were separated, and any region smaller than

Figure 1. Schematic. *A*: first, the high-resolution connectome is computed from the pairwise correlations of the BOLD time course of each vertex. The pictured timeseries are randomly generated. Connectomes are calculated on an individual level. The group-average connectome of 500 random subjects is pictured. Second, from this group-level connectome, *k*-means is run from $k = 2$ to 200 clusters to define group-level parcellations. Third, individual-level parcellations are calculated for the remaining 518 subjects using k-nearest neighbor's classification (*k*-NN). Three subject's parcellations are shown for the $k = 7$ parcellation. *B*: in the training stage, an individual's actual fROI (task-fROI) is matched to all resting state parcellations (from $k = 2$ to $k = 200$ networks). For each subject in the $n = 500$ training set, a task-fROI is defined from the task data using the group-constrained search space method (26). Then, the dice overlap is computed between that individual's task-fROI and all networks (e.g., network 1 to *k* in each *k*-parcellation) within each *k*-resting state parcellation. The final rs-fROI that will be applied to the test set is selected by finding the network with the highest dice across all subjects and parcellations. For example, the identified rs-fROI for the Left Hand (LH) fROI is network #53 from the $k = 198$ network resting state parcellation. *C*: then, for each subject in the testing group ($n = 518$), the rs-fROI is computed using only the resting state data. From an individual's resting state connectome, each vertex is assigned to a given network using *k*-nearest neighbor classification based on similarity of its functional connectivity to the centroids of the *k*-parcellation identified in the training stage (e.g., $k = 198$ for LH). Then, the rs-fROI for that individual is computed by selecting the top network identified in the training stage (e.g., network #53 from $k = 198$). Note that the rs-fROIs identified in the testing group are computed using only that individual's resting state functional connectivity. fROI, functional region of interest; rs, resting state.

500 mm^2 was excluded. An insula component for the left foot – average contrast was not included. Finally, the remaining components were dilated on the surface with a distance of 5mm^2 kernel to provide a large enough search space to ensure we can reliably identify fROIs in individual subjects.

The language and vision search spaces were defined from external sources. The language search spaces were downloaded from the Fedorenko Lab localizers (https://evlab.mit.edu/funcloc/) and consisted of six parcels originally reported in Fedorenko et al. (26). We used the "updated" version of these parcels, which contained data from a total of 220 individuals. The visual category-selective search spaces came from a similar approach by Julian et al. (23). All search spaces, including the motor and working memory search spaces described earlier, are shown in Fig. 2. The task fROI was then defined by masking an individual subject's task activation within the search space. Namely, individual task fROIs for a given contrast were defined as any vertex within a specific search space where $P < 0.05$ for the appropriate contrast.

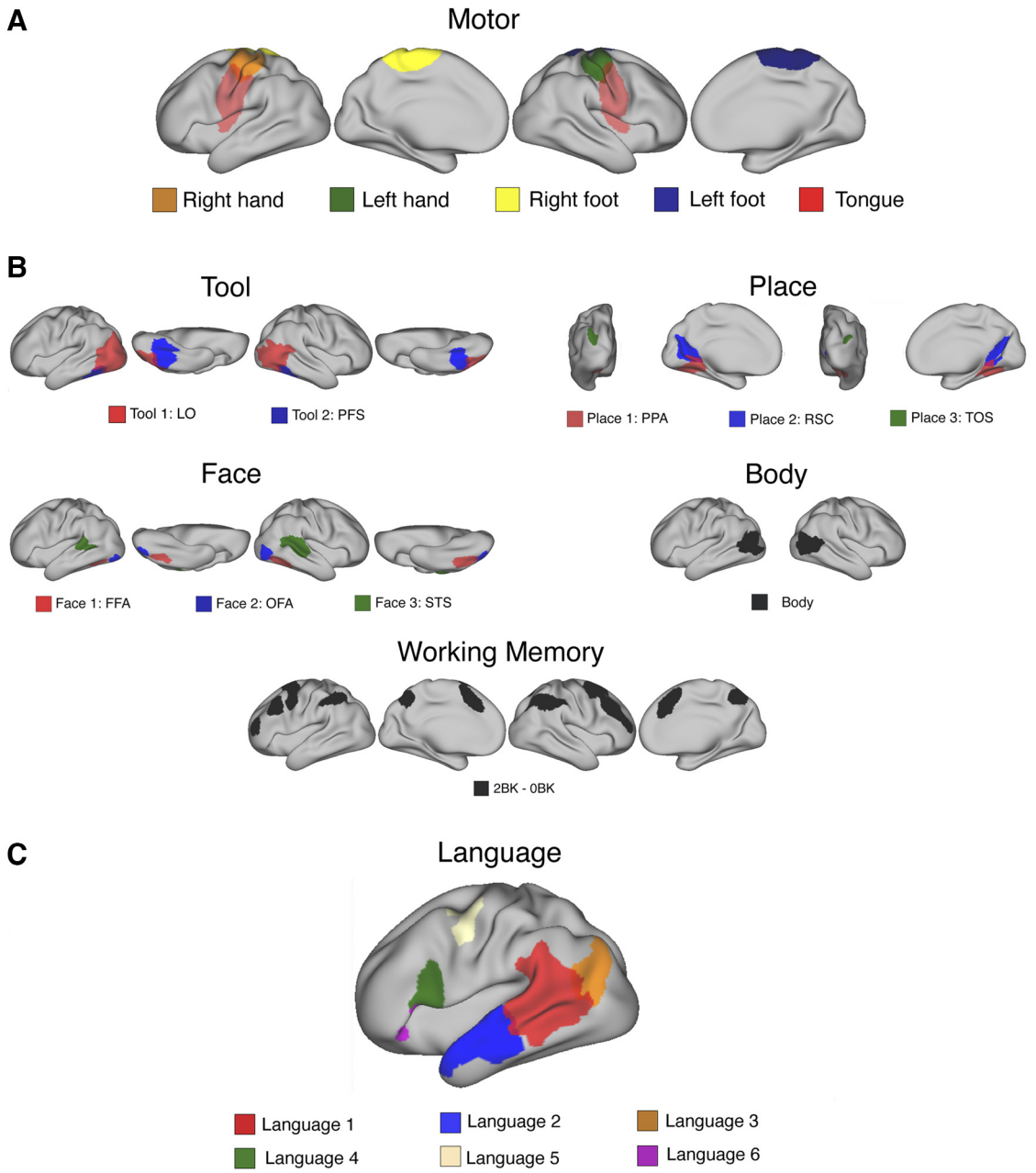

Figure 2. Search spaces for functional regions of interest (fROIs). *A*: the motor search spaces are identified for each body part (e.g., right hand – the average of all others is identified in red). *B*: for the working memory task, five contrasts were used to localize activity related to tools, places, faces, bodies, and working memory. Three contrasts included multiple search spaces and those different components are separated by color: tool includes lateral occipital (*tool 1*: LO) and posterior fusiform sulcus (*tool 2*: PFS); place includes parahippocampal place area (*place 1*: PPA), retrosplenial cortex (*place 2*: RSC), and transverse occipital sulcus (*place 3*: TOS); and face includes fusiform face area (*face 1*: FFA), occipital face area (*face 2*: OFA), and superior temporal sulcus (*face 3*: STS). *C*: in the language comprehension task, the six different search spaces were obtained from Fedorenko et al. (26).

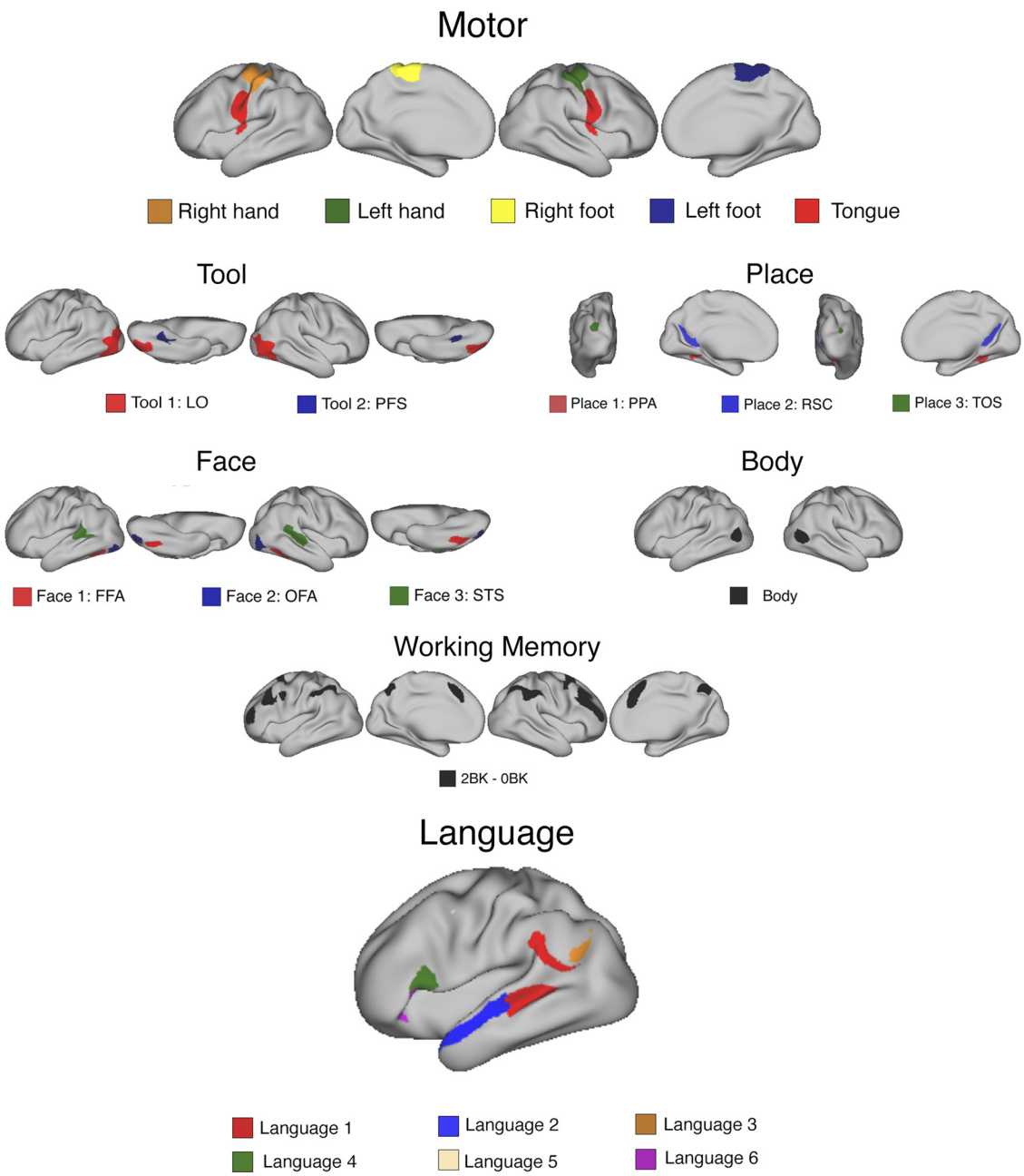

Figure 3. Resting state (rs)-fROIs. The identified functional regions of interest constructed from resting state functional connectivity (i.e., rs-fROIs) with the highest overlap with a given contrast/search space in the motor task, working memory task, and language task are plotted on the surface for each putative fROI. The motor rs-fROIs are identified for each body part (e.g., right hand – the average of all others is identified in red). For the working memory task, five contrasts were used to localize activity related to tools, places, faces, bodies, and working memory. Three contrasts included multiple search spaces and those different components are separated by color: tool includes lateral occipital (*tool 1*: LO) and posterior fusiform sulcus (*tool 2*: PFS); place includes parahippocampal place area (*place 1*: PPA), retrosplenial cortex (*place 2*: RSC), and transverse occipital sulcus (*place 3*: TOS); and face includes fusiform face area (*face 1*: FFA), occipital face area (*face 2*: OFA), and superior temporal sulcus (*face 3*: STS). In the language comprehension task, only one contrast was used (Story – Math), but six different components were localized using search spaces from Fedorenko et al. (26). fROI, functional region of interest.

For every contrast and every subject in the training group of 500, we calculated the overlap (quantified using the dice coefficient) between a given task fROI and every individualized resting state cluster (network) for all parcellations. Associated group-level resting state networks were identified by finding the network with the highest mean overlap across the training group. The final matched network was masked by the search space to create the rs-fROI.

rs-fROI Test Group

In the remaining 518 individuals, rs-fROIs were defined by computing individualized resting state parcellations for all k total networks defined in the training stage. Then, for a given fROI, the matched network number was selected and masked by the search space to define an rs-fROI. To validate that rs-fROIs were indeed selective for the expected category,

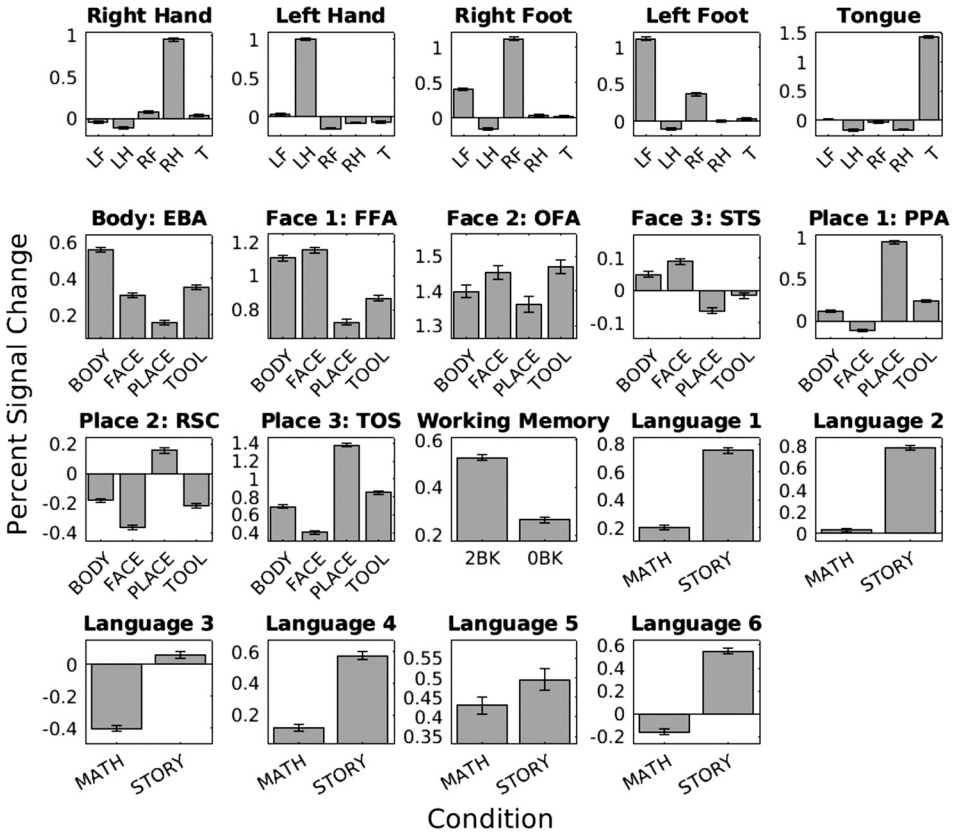

Figure 4. Selectivity of rs-fROIs. Each panel shows the percent signal change for all conditions of interest within a putative functional region of interest. The height of the bar shows the mean percent signal change, and the error bars show the standard error of the mean. FFA, fusiform face area; fROI, functional region of interest; LO, lateral occipital; OFA, occipital face area; PFS, posterior fusiform sulcus; PPA, parahippocampal place area; rs, resting state; RSC, retrosplenial cortex; TOS, transverse occipital sulcus.

we computed selectivity in each region for the 518 individuals in the test group. We report the mean percent signal change (PSC) for each condition in each task. For the motor regions, the contrast category was the mean of all of the other categories (e.g., selectivity for the right-hand region was based on the PSC of the right hand − the average PSC of the left hand, right foot, left foot, and tongue). For the high-level visual regions (preferred categories of faces, bodies, or scenes), the contrast was the PSC response to tools. The tool regions (LO and PFS) are excluded from this analysis, as there was no scrambled tool category (23, 41). Finally, the contrasts for the working memory region and language comprehension regions were 2-back versus 0-back and story versus math, respectively. Significant selectivity was assessed using a two-sided paired *t* test with the alternate hypothesis that the PSC of the expected category was different than the PSC of the contrast category. The same procedure for computing and validating rs-fROIs was followed in the 28 retest individuals. Note that rs-fROIs were computed for all four connectomes (from 15 min of data) per retest individual, then the PSCs for each category were averaged within the individual across the four runs.

Finally, we explored whether these individualized rs-fROIs exhibit higher selectivity than group-level probabilistic atlas parcels. First, we compared the selectivity of the search spaces described above (Fig. 2) to our identified rs-fROIs. Second, we compare the rs-fROIs to three atlases developed for functional modules across motor control, language, and vision. These atlases are the hand motor area atlas (HAMOTA) of regions involved in motor control of the hand (47), the visual functional atlas (visfAtlas) which includes category-selective regions (48), and the sentence supramodal areas atlas (SENSAAS) of language, specifically sentence processing (9).

Parcels from these atlases were matched to a putative fROI based on overlap with the appropriate search space. For HAMOTA, the left-hand fROI (on the left hemisphere) was matched to prec6 (S_precentral-6), rol2 (S_rolando-2), rol3 (S_rolando-3), rol4 (S_rolando-4), and post2 (S_rostcentral-2); and the left-hand fROI (on the right hemisphere) was matched to the right hemispheric versions of those same regions. For the visfAtlas, the following fROIs were matched to these corresponding parcels: the FFA includes the midlateral fusiform gyrus (mFus) and posterior lateral fusiform gyrus (pFus); the OFA includes the bilateral inferior occipital gyrus (IOG); the EBA includes the bilateral inferior temporal gyrus (ITG), middle temporal gyrus (MTG), and lateral occipital sulcus (LOS); the PPA includes the bilateral collateral sulcus (COS); and the TOS includes the right transverse occipital sulcus (rhTOS). Finally, for SENSAAS, the language fROIs were matched to these corresponding parcels: *language 1* includes SMG7 (G_supramarginal-7), STS3 (S_sup_temporal-3), STS4 (S_sup_temporal-4), T2_3 (G_temporal_mid-3), and T2_4 (G_temporal_mid-4); *language 2* includes T1_4 (G_temporal_Sup-4), STS1 (S_sup_temporal-1), and STS2 (S_sup_temporal-2); *language 3* includes AG2 (G_angular-2); *language 4* includes f2_2 (S_inf_frontal-2) and F3t (G_frontal_inf_tri-1); *language 5* includes prec4 (S_precentral-4); and *language 6* includes F3O1 (G_frontal_inf_orb-1), INSa2 (G_insula-anterior-2), and INSa3 (G_insula-anterior-3). Note that all these regions are part of the core sentence processing network (SENT_CORE).

In all comparisons of our rs-fROIs to matched atlas parcels and search spaces, significance was assessed using a two-

sided paired t-test with the alternate hypothesis that the mean selectivity of the rs-fROI is different than the mean selectivity of the search space or atlas parcels. Bonferroni–Holm corrections (49) are used throughout to access significance, but *P* values presented in all tables are the raw uncorrected *P* values. A positive T-statistic indicates the mean selectivity is higher for the rs-fROI.

RESULTS

Identifying rs-fROIs

First, we identified rs-fROIs constructed from individualized resting state functional connectivity parcellations corresponding to putative fROIs for motion, working memory, high-level vision, and language comprehension (Fig. 3). In the training set of 500 individuals, we searched through every network in every parcellation resolution (from 2 to 200 networks) and calculated the overlap between that individual's resting state network in the parcellation and their task-fROI (i.e., defined from their task data). Note that because the individual parcellations are computed from group centroids, the network labels are consistent across individuals (e.g., network #5 in the $k = 30$ network parcellation is considered to be the same network for every subject). Then, the rs-fROI is defined by the overlapping region of the best matching networks and the search space.

We identified rs-fROIs for five motor regions (for right hand, left hand, right foot, left foot, and tongue), a distributed working memory network (defined using the contrast 2-back–0-back in the embedded n-back task), nine high-level visual regions [3 place regions, 3 face regions, 2 tool regions, and 1 body region; Julian et al. (23)], and six language regions [from Fedorenko et al. (26)]. The matched region's *k* resolution and network number are listed in Supplemental Table S1. For example, the network that was found to best approximate the PPA was cluster #139 in the $k = 167$ network parcellation. These rs-fROIs can be identified for new out-of-sample subjects using the centroids identified in the group-level parcellation. In Fig. 3, note the group-level rs-fROIs (defined from the group parcellation of 500 individuals) are plotted, but the individualized versions of these rs-fROIs are used for the following analyses.

Selectivity of rs-fROIs

Next, we determined the selectivity of these rs-fROIs in the remaining 518 individuals. Note that we only compared fROIs that we could extract selectivity from, given the HCP task data [tool regions were excluded due to the absence of a scrambled tool/object condition; Barch et al. (40), Julian et al. (23)]. Figure 4 shows the average percent signal change (PSC) for each condition. If a given rs-fROI is deemed selective for its preferred condition, then the PSC for that condition would be significantly greater than the PSC for its most standard contrast condition. Based on the mean PSCs shown in Fig. 4, this is the case for nearly every rs-fROI. To determine if selectivity was observed on an individual level, selectivity was quantified as the difference between the PSC of the expected preferred category minus the PSC of the contrast category (i.e., for motor fROIs, the contrast category is the average of all non-preferred categories; for the high-level vision fROIs, the contrast category is tools; see MATERIALS AND METHODS). The *P* values for each rs-fROI are listed in Table 1. Note that a few individuals did not have any fMRI data for a given task, resulting in different degrees of freedom. After accounting for multiple comparisons with a Bonferroni–Holm correction, all rs-fROIs were significantly selective for their category of interest.

To explore if shorter resting state runs still yield selective rs-fROIs, we computed rs-fROIsv for a retest subset of 28 of the 518 individuals who were scanned again within a year of the original visits. Instead of using the full 60-min resting state data, concatenated across four runs, we instead only used single 15-min runs. The *P* values for the selectivity of the rs-fROIs defined using shorter resting state runs for each fROI are listed in Table 2 (note that 1 individual did not have data for the language comprehension task). All regions exhibited significant selectivity for the expected category, except for *language 5* (Bonferroni–Holm corrected *P* value = 0.975), and the OFA (Bonferroni–Holm corrected *P* value = 0.397). As this duration of resting state data is more congruent with the scanning protocols in most laboratories, this substantiates the plausibility of using only resting state data to define selective fROIs in a typical research setting.

Comparison to Probabilistic Atlas Parcels

However, is this selectivity better than the selectivity of group-level probabilistic parcels? Generating individualized resting state functional parcellations is time-consuming and computationally demanding, so we tested if the rs-fROIs outperformed the search spaces (23, 26, 41) or parcels from atlases specifically developed for functional modules including the hand motor area atlas (HAMOTA) of regions involved in motor control in the hand (47), the visual functional atlas (visfAtlas) which includes category-selective regions (48), and the sentence supramodal areas atlas (SENSAAS) of language, specifically sentence processing (9). We used the same

Table 1. *Selectivity of personalized rs-fROIs*

Putative fROI	rs-fROI Selectivity (*P* Value)	*T* Statistic
Right hand	5.36×10^{-219}	$T(514) = 55.44$
Left hand	2.12×10^{-241}	$T(514) = 62.21$
Right foot	1.57×10^{-223}	$T(514) = 56.76$
Left foot	1.48×10^{-225}	$T(514) = 57.36$
Tongue	2.47×10^{-301}	$T(514) = 83.58$
Body: EBA	3.13×10^{-140}	$T(513) = 35.49$
Face 1: FFA	3.30×10^{-50}	$T(513) = 16.68$
Face 2: OFA	0.000677	$T(513) = 3.42$
Face 3 STS	1.32×10^{-46}	$T(513) = 15.91$
Place 1: PPA	1.87×10^{-209}	$T(513) = 52.78$
Place 2: RSC	1.81×10^{-120}	$T(513) = 31.17$
Place 3: TOS	5.32×10^{-220}	$T(513) = 55.8$
Working memory	3.62×10^{-61}	$T(513) = 18.96$
Language 1	1.79×10^{-177}	$T(511) = 44.39$
Language 2	2.11×10^{-216}	$T(511) = 54.89$
Language 3	1.94×10^{-107}	$T(511) = 28.46$
Language 4	3.01×10^{-97}	$T(511) = 26.34$
Language 5	4.98×10^{-5}	$T(511) = 4.09$
Language 6	2.28×10^{-155}	$T(511) = 39.02$

P values computed from a two-sided paired *t* test. Body: EBA, extrastriate body area; face 1: FFA, fusiform face area; face 2: OFA, occipital face area; face 3: STS, superior temporal sulcus; fROI, functional region of interest; place 1: PPA, parahippocampal place area; place 2: RSC, retrosplenial cortex; place 3: TOS, transverse occipital sulcus; rs, resting state.

Table 2. *Selectivity of personalized rs-fROIs from 15-min resting state scans*

Putative fROI	rs-fROI Selectivity (*P* Value)	*T* Statistic
Right hand	5.16×10^{-15}	$T(27) = 15.57$
Left hand	2.71×10^{-14}	$T(27) = 14.54$
Right foot	1.01×10^{-13}	$T(27) = 13.76$
Left foot	2.68×10^{-14}	$T(27) = 14.55$
Tongue	1.16×10^{-18}	$T(27) = 21.78$
Body: EBA	3.11×10^{-8}	$T(27) = 7.65$
Face 1: FFA	0.00896	$T(27) = 2.82$
Face 2: OFA	0.397	$T(27) = -0.86$
Face 3 STS	0.00265	$T(27) = 3.31$
Place 1: PPA	2.30×10^{-8}	$T(27) = 7.78$
Place 2: RSC	1.11×10^{-4}	$T(27) = 4.52$
Place 3: TOS	1.50×10^{-10}	$T(27) = 9.98$
Working memory	2.50×10^{-7}	$T(27) = 6.82$
Language 1	1.64×10^{-9}	$T(26) = 9.05$
Language 2	2.90×10^{-14}	$T(26) = 14.92$
Language 3	3.92×10^{-5}	$T(26) = 4.94$
Language 4	2.57×10^{-4}	$T(26) = 4.23$
Language 5	0.975	$T(26) = 0.03$
Language 6	1.98×10^{-12}	$T(26) = 12.41$

P values computed from a two-sided paired *t* test. Body: EBA, extrastriate body area; face 1: FFA, fusiform face area; face 2: OFA, occipital face area; face 3: STS, superior temporal sulcus; fROI, functional region of interest; place 1: PPA, parahippocampal place area; place 2: RSC, retrosplenial cortex; place 3: TOS, transverse occipital sulcus; rs, resting state.

definition of selectivity as above for our comparisons, and the results are summarized in Table 3. For the search spaces, the selectivity of nearly every fROI improved when using the individualized resting state rs-fROIs. The OFA was the only region where the search space parcel had significantly higher mean selectivity (mean difference = −0.0164; Bonferroni–Holm corrected *P* value = 0.0298). For the visfAtlas, five high-level visual areas were compared (see MATERIALS AND METHODS for additional details). Again, all regions except for the OFA showed higher selectivity in the individualized rs-fROIs. Here, the difference between the rs-fROIs and probabilistic parcels (mean = −0.0885) was still significant after correcting for multiple comparisons indicating the atlas method is preferred for this region (corrected *P* value = 6.84×10^{-15}). Parcels from the HAMOTA atlas were compared with the bilateral hand rs-fROIs, and the selectivity of both rs-fROIs was significantly higher than the group-level HAMOTA parcels. Finally, parcels from the SENSAAS atlas were compared with the six language rs-fROIs, and we found the rs-fROIs had significantly higher selectivity than the SENSAAS parcels in this case as well.

Characterizing Parcellations

The identified rs-fROIs are derived from multiple resolutions of resting state data. Our final analyses explore how the resting state networks varied from $k = 2$ to 200 networks. Overall, the group-level parcellations yielded symmetric networks with high spatial continuity, despite the high-resolution and high-dimensionality of the connectome. These are features expected from functional networks, but importantly, this information appears to be preserved in the functional data alone without structural or hemispheric constraints.

Figure 1 shows the two extremes of these group-level results ($k = 2$ networks and $k = 200$ networks) plotted on the surface. All parcellations are plotted on the lateral surface in Supplemental Fig. S1, where the number of networks increases from 2 to 200. We were particularly interested in areas of the cortex that remained a single network or were often a transition point between networks, across all of the parcellations. To quantify this we computed the number of parcellations where a given vertex was a boundary (Fig. 5*A*). The boundaries of many clusters do not drastically change, and well-defined sensorimotor and visual clusters are

Table 3. *Comparison of personalized rs-fROIs to probabilistic parcels*

	Search Spaces		Atlases	
Putative fROI	*P* Value	*T* Statistic	*P* Value	*T* Statistic
Right hand	1.84×10^{-122}	$T(514) = 31.58$	3.28×10^{-156}	$T(514) = 39.12^{a}$
Left hand	3.66×10^{-131}	$T(514) = 33.46$	9.79×10^{-193}	$T(514) = 48.18^{a}$
Right foot	2.15×10^{-130}	$T(514) = 33.29$		
Left foot	1.78×10^{-144}	$T(514) = 36.42$		
Tongue	1.39×10^{-250}	$T(514) = 65.16$		
Body: EBA	1.04×10^{-46}	$T(513) = 15.93$	3.79×10^{-6}	$T(513) = 4.67^{b}$
Face 1: FFA	1.61×10^{-9}	$T(513) = 6.15$	0.000117	$T(513) = 3.88^{b}$
Face 2: OFA	0.0298	$T(513) = -2.18$	1.71×10^{-15}	$T(513) = -8.22^{b}$
Face 3 STS	9.75×10^{-24}	$T(513) = 10.56$		
Place 1: PPA	3.16×10^{-124}	$T(513) = 31.98$	4.39×10^{-10}	$T(513) = 6.36^{b}$
Place 2: RSC	1.04×10^{-119}	$T(513) = 31.01$		
Place 3: TOS	2.00×10^{-74}	$T(513) = 21.67$	5.96×10^{-75}	$T(513) = 21.78^{b}$
Working memory	2.23×10^{-56}	$T(513) = 17.97$		
Language 1	1.59×10^{-188}	$T(511) = 47.22$	3.91×10^{-162}	$T(511) = 40.62^{c}$
Language 2	6.90×10^{-71}	$T(511) = 20.97$	2.36×10^{-88}	$T(511) = 24.52^{c}$
Language 3	2.96×10^{-82}	$T(511) = 23.28$	1.66×10^{-135}	$T(511) = 34.49^{c}$
Language 4	2.65×10^{-67}	$T(511) = 20.23$	3.24×10^{-104}	$T(511) = 27.78^{c}$
Language 5	3.43×10^{-69}	$T(511) = 20.62$	4.19×10^{-26}	$T(511) = 11.18^{c}$
Language 6	1.08×10^{-6}	$T(511) = 4.94$	1.83×10^{-207}	$T(511) = 52.35^{c}$

P values computed from a two-sided paired *t* test. Body: EBA, extrastriate body area; face 1: FFA, fusiform face area; face 2: OFA, occipital face area; face 3: STS, superior temporal sulcus; fROI, functional region of interest; place 1: PPA, parahippocampal place area; place 2: RSC, retrosplenial cortex; place 3: TOS, transverse occipital sulcus; rs, resting state. [a]Atlas parcel from hand motor area atlas (HAMOTA; 47); [b]atlas parcel from visual functional atlas (visfAtlas; 48); [c]atlas parcel from sentence supramodal areas atlas (SENSAAS; 9).

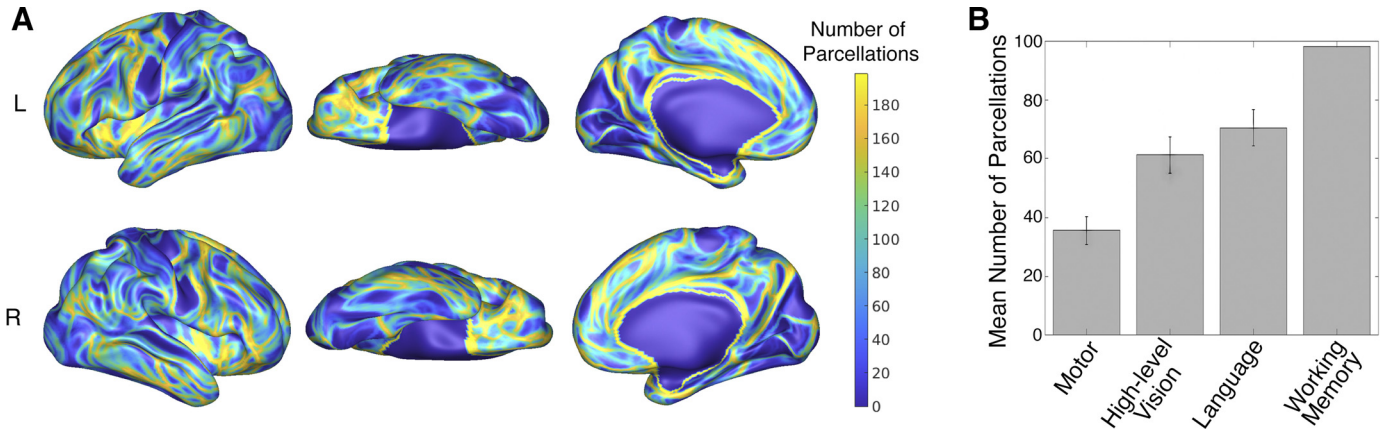

Figure 5. Number of times vertices are boundaries. *A*: yellow colors indicate if a vertex is a boundary between networks for all the *k* network parcellations from $k = 2$ to 200 (maximum of 199 parcellations). Blue colors indicate areas where vertices are never separated into different networks. *B*: the mean number of parcellations where vertices are boundaries was computed within each rs-fROI. The bar plot shows the average across rs-fROIs for each domain, with the error bars indicating the standard error of the mean. fROI, functional region of interest; rs, resting state.

particularly preserved across the parcellations, e.g., rarely if ever are subdivided into smaller clusters.

Are the rs-fROIs we defined preserved across all possible total networks? To explore this question, we quantified how often vertices within a rs-fROI (from Fig. 3) are boundaries. The mean within a rs-fROI indicates if the region comprises many transition points, i.e., is often subdivided across the different resolutions. A lower value indicates a module of cortex that is more stable across resolutions, or not often a border as the *k* total networks change. Figure 5*B* shows the mean number of times vertices are a boundary, averaging across domains. Consistent with the whole brain results in Fig. 5*A*, the motor rs-fROIs were found to be the most stable, followed by high-level vision rs-fROIs, then language rs-fROIs, and the working memory rs-fROIs were the most divisible.

DISCUSSION

Here, we demonstrate that individualized networks defined from only resting state functional connectivity ("rs-fROIs") are capable of identifying an individual's own functional regions of interest (fROIs) for motion, high-level vision, working memory, and language comprehension. These rs-fROIs were defined as the network (across an entire sequence of parcellations from 2 to 200 networks) that most closely matched the task-defined individual fROI ("task-fROI") in a training group of 500 individuals. Critically, in an independent test set of 518 individuals, all rs-fROIs were indeed selective for their appropriate preferred condition. Nearly all fROIs were significantly more selective when defined by the rs-fROIs than when defined by probabilistic group atlases.

Individualized rs-fROIs showed significant selectivity for all fROIs. Even when only using a fraction of the available data, rs-fROIs computed from 15 min of resting state data were still significantly selective for nearly all fROIs, with the exception of one language and face region (*language 5* and the OFA). These results establish the potential of using resting state functional connectivity as a tool for predicting fROIs, without the need for an additional localizer scan, complementing previous work using structural connectivity to predict high-level visual fROIs (50, 51). Moreover, the selectivity of the rs-fROIs corroborates evidence revealing a close link between connectivity and brain activity (16–18, 52). Using a single resting state scan, as opposed to multiple localizer tasks, has the practical advantage of saving time, research funding, and effort while scanning. Our code will be publicly available to allow researchers to compute rs-fROIs from their own resting state data.

The OFA rs-fROI did not show higher selectivity than probabilistic atlas parcels, potentially because it was defined by faces – average, instead of the typical faces – objects definition (23). Alternatively, the specific localizer task may not have been ideal for capturing all face selective regions, because *1*) there were only two runs, *2*) some regions involved in face processing (including the OFA) elicit higher responses to faces using dynamic, as opposed to static stimuli (53), and *3*) because the task was designed within a larger two-back memory task. Future work will address these points by using datasets that more precisely map responses to high-level visual categories, but here we found that using Julian et al.'s (23) search space, or particularly, the IOG parcel from the Rosenke et al. (48) atlas yielded more selective fROIs than the individualized rs-fROI for the OFA. We were further limited by the lack of available data to localize the tool regions (LO and PFS) as there was no scrambled objects condition, a necessary contrast to identify these regions (23). Finally, although other task domains are available from the HCP (41), we did not include them because there was very little overlap across subjects. Future work could explore whether resting state rs-fROIs can estimate fROIs in other domains, e.g., low-level vision or networks involved in theory of mind.

We computed and investigated an entire sequence of parcellations, but we do not propose the use of any single parcellation as the optimal parcellation for all purposes. The ideal parcellations depend on the researcher's goal and question of interest. For example, if a researcher was interested in high-level vision, a low-resolution parcellation that contains broad-scale networks would not include smaller components of those networks such as the FFA or PPA. Conversely, for broad-scale organization comparisons (e.g., comparing working memory networks on an individual

level), a lower-resolution parcellation would be preferred. Likely, multiple parcellations would be appropriate, as even within a given domain (e.g., language) there was not a single k network parcellation that best captured every fROI (see Supplemental Table S1). This is in line with previous work releasing atlases across a range of resolutions [such as Dadi et al. (54)] and advocating that there is no single parcellation that is appropriate for all applications (4, 35, 55).

Due to the ubiquity of individual differences in psychology and neuroscience, many researchers have proposed methods to generate individual parcellations based on functional connectivity (6, 10, 36–38, 56–59). Personalized parcellations not only better represent the underlying connectivity but they also better predict an individual's behavior (10, 60). Our approach differs from existing individual parcellations for two main reasons. First, as described earlier, our approach does not assume a single parcellation and reports rs-fROIs from parcellations across an entire sequence of resolutions. We identify potential parcellations to adopt for each fROI separately based on the training data's resting state network and task-fROI overlap. Because our approach is group-informed with consistent labels (e.g., network #1 will be #1 in all subjects), a given fROI can be approximated for any out-of-sample subject (e.g., to approximate their OFA, we personalize the $k = 106$ network parcellation and select the network #21). Second, the underlying connectivity data used here to define the connectomes is on a vertex level and does not impose any spatial constraints. Previous approaches either *1*) first reduced the connectome using PCA (57), *2*) averaged seed and/or targets defined by previous parcellations (37, 38, 56, 58), or *3*) downsampled the surface to small ROIs (10, 36). This is advantageous because it limits the number of experimenter assumptions in preprocessing the data allowing for a fully data-driven approach. Other approaches were also spatially constrained, e.g., utilized gradient-based parcellation to find boundaries between spatially continuous parcels (6, 59), followed a region growing approach (36), or incorporated a spatial prior to ensure neighboring vertices are more likely to be assigned together (10, 37). Although these assumptions are reasonable and often useful for defining functional nodes, our approach is completely data driven and aims to uncover networks from functional connectivity alone. Despite the lack of spatial assumptions, we observed that spatially continuous networks still emerge both across the group and within an individual even when these constraints are removed.

Furthermore, in the absence of any spatial or down-sampling constraints, many boundaries were stable across resolutions, especially in primary sensory and motor cortices. These regions are likely the most simple and coarsest natural processing units. The fact the regions are not broken up frequently suggests modularity and homogenous connectivity profiles within that area of the cortex. Accordingly, motor rs-fROIs were the most stable across parcellations compared to the other domains. High-level visual and language rs-fROIs showed similar levels of stability but were subdivided in other resolutions more than the motor rs-fROIs. The working memory rs-fROI tended to be the most subdivided and comprises multiple distributed regions in association cortices. Additionally, the working memory network functions include many combinations of distinct and interacting cognitive processes (61). From the inclusion of multiple regions and broad function of the working memory network, it follows that this rs-fROI is less modular in its connectivity profile when compared with, e.g., the right-hand rs-fROI. Future investigations should explore the distinct functions of subunits within these broad rs-fROIs.

Although the lack of spatial constraints is advantageous for allowing a fully data-driven approach, this can also be a limitation because it does not explicitly model known features of the human brain. First, for example, a defining feature of the brain is homotopy, i.e., the characteristic symmetry across hemispheres (62, 63). Homotopic atlases computed from functional connectivity also show reduced task inhomogeneity compared with nonhomotopic atlases across a variety of tasks and datasets (64). However, for our purposes, homotopic atlases would not be able to capture hemispheric differences in, e.g., the right and left FFA. Another advantage of a homotopic atlas is that it allows investigations into lateralization. Lateralization is of particular interest for researchers interested in, e.g., handedness and individual differences in hemispheric dominance of the language network (65). Other group-level atlases that incorporate homotopy (64, 66) would be more appropriate for answering questions about individual differences in lateralization. Second, our parcellation only includes resting state data and does not incorporate task data in the definition of the individualized parcellations. Multi-modal approaches, such as publicly available group-level atlases that include task and/or structural data in addition to functional connectivity (54, 67), have the advantage of combining the unique strengths of different neuroimaging modalities. However, we chose to define atlases without including any task data, to explore the feasibility of using only resting state data to define individual specific fROIs across different domains, potentially circumventing the need for multiple localizer task scans saving time and resources.

The rs-fROIs and parcellations here were determined based on a large sample of young adults, and it is unclear if these results are suitable or would generalize to younger cohorts. This is mainly because adults and children have characteristically different patterns of functional connectivity (68, 69). However, many of these fROIs can be identified very early on. For example, motor fROIs are present early in life, as a contralateral hand fROI appears as early as infancy (70). High-level visual fROIs have also been localized in infants (71), and the organization of occipitotemporal cortex can be explained by gene expression (72). Other fROIs may require experience, so they may be unidentifiable in younger age groups. For example, the visual word form area requires knowledge of reading. However, there still appears to be a close relationship between these fROIs and connectivity, as structural connectivity can be used to identify the future location of this region (73). Additionally, even within the same domain (e.g., scene processing), different fROIs supporting distinct aspects of processing, may develop at varying rates (33). Finally, a multitude of studies have documented differences in functional connectivity related to psychological disorders (74). The parcellations presented here may then also be unsuitable for clinical populations. Although the networks and centroids presented here may not be ideal for developing and clinical populations, they could be used as a starting point and updated based on new group or individual connectomes. Future work could explore

the relationship between connectivity patterns and fROIs in developing and clinical populations.

Conclusions

Using a large sample of young adult data from the Human Connectome Project, we identify individualized resting state connectivity rs-fROIs that best capture an individual's function regions of interest (fROIs) across domains including motor control, language comprehension, working memory, and high-level vision. These regions are derived from group-informed data-driven parcellations for a single individual based on vertex-to-vertex functional connectivity. Critically, the rs-fROIs show expected selectivity and outperform probabilistic atlas parcels. Overall, this provides a potential method for defining individual fROIs without task data. Finally, we release code to allow researchers to apply the individualized parcellations and use their own resting state data to define individualized fROIs.

DATA AVAILABILITY

The neuroimaging data used in this study are available as part of the publicly available Human Connectome Project (HCP; http://www.humanconnectomeproject.org/). Group-level parcellations and centroids are publicly available at https://github.com/CognitionBrainCircuitryLab/PersonalizedAtlas. Analyses were completed using MATLAB R2020a (The MathWorks Inc., Natick, MA). MATLAB code to calculate individual parcellations is publicly available (https://github.com/CognitionBrainCircuitryLab/PersonalizedAtlas). All code is available from the authors upon request.

SUPPLEMENTAL DATA

All Supplemental material is available at https://doi.org/10.5281/zenodo.8061346.

ACKNOWLEDGMENTS

The authors thank Z.M. Saygin for helpful feedback. We acknowledge the Ohio Supercomputer Center (www.osc.edu) for their computational resources and support.

GRANTS

Data were provided by the Human Connectome Project, WU-Minn Consortium (Principal Investigators: David Van Essen and Kamil Ugurbil; 1U54MH091657) funded by the 16 National Institutes of Health (NIH) Institutes and Centers that support the NIH Blueprint for Neuroscience Research; and by the McDonnell Center for Systems Neuroscience at Washington University. This research was partially funded by The Ohio State University's College of Arts and Sciences. M.F. Molloy was supported by F31 HD107961. Analyses were completed using the Ohio Supercomputer (https://www.osc.edu).

DISCLOSURES

No conflicts of interest, financial or otherwise, are declared by the authors.

AUTHOR CONTRIBUTIONS

M.F.M. and D.E.O. conceived and designed research; M.F.M. and D.E.O. analyzed data; M.F.M. and D.E.O. interpreted results of experiments; M.F.M. prepared figures; M.F.M. drafted manuscript; M.F.M. and D.E.O. edited and revised manuscript; M.F.M. and D.E.O. approved final version of manuscript.

REFERENCES

1. **Brodmann K.** *Vergleichende Lokalisationslehre der Grosshirnrinde in ihren Prinzipien dargestellt auf Grund des Zellenbaues*. Leipzig, Germany: Barth, 1909.
2. **Makris N**, **Goldstein JM**, **Kennedy D**, **Hodge SM**, **Caviness VS**, **Faraone SV**, **Tsuang MT**, **Seidman LJ.** Decreased volume of left and total anterior insular lobule in schizophrenia. *Schizophr Res* 83: 155–171, 2006. doi:10.1016/j.schres.2005.11.020.
3. **Dickie DA**, **Shenkin SD**, **Anblagan D**, **Lee J**, **Blesa Cabez M**, **Rodriguez D**, **Boardman JP**, **Waldman A**, **Job DE**, **Wardlaw JM.** Whole brain magnetic resonance image atlases: a systematic review of existing atlases and caveats for use in population imaging. *Front Neuroinform* 11: 1, 2017. doi:10.3389/fninf.2017.00001.
4. **Eickhoff SB**, **Yeo BTT**, **Genon S.** Imaging-based parcellations of the human brain. *Nat Rev Neurosci* 19: 672–686, 2018. doi:10.1038/s41583-018-0071-7.
5. **Betzel RF**, **Byrge L**, **He Y**, **Goñi J**, **Zuo XN**, **Sporns O.** Changes in structural and functional connectivity among resting state networks across the human lifespan. *NeuroImage* 102: 345–357, 2014. doi:10.1016/j.neuroimage.2014.07.067.
6. **Gordon EM**, **Laumann TO**, **Gilmore AW**, **Newbold DJ**, **Greene DJ**, **Berg JJ**, **Ortega M**, **Hoyt-Drazen C**, **Gratton C**, **Sun H**, **Hampton JM**, **Coalson RS**, **Nguyen AL**, **McDermott KB**, **Shimony JS**, **Snyder AZ**, **Schlaggar BL**, **Petersen SE**, **Nelson SM**, **Dosenbach NUF.** Precision functional mapping of individual human brains. *Neuron* 95: 791–807.e7, 2017. doi:10.1016/j.neuron.2017.07.011.
7. **Fan L**, **Li H**, **Zhuo J**, **Zhang Y**, **Wang J**, **Chen L**, **Yang Z**, **Chu C**, **Xie S**, **Laird AR**, **Fox PT**, **Eickhoff SB**, **Yu C**, **Jiang T.** The human brainnetome atlas: a new brain atlas based on connectional architecture. *Cereb Cortex* 26: 3508–3526, 2016. doi:10.1093/cercor/bhw157.
8. **Hesling I**, **Labache L**, **Joliot M**, **Tzourio-Mazoyer N.** Large-scale plurimodal networks common to listening to, producing and reading word lists: an fMRI study combining task-induced activation and intrinsic connectivity in 144 right-handers. *Brain Struct Funct* 224: 3075–3094, 2019. doi:10.1007/s00429-019-01951-4.
9. **Labache L**, **Joliot M**, **Saracco J**, **Jobard G**, **Hesling I**, **Zago L**, **Mellet E**, **Petit L**, **Crivello F**, **Mazoyer B**, **Tzourio-Mazoyer N.** A SENtence Supramodal Areas AtlaS (SENSAAS) based on multiple task-induced activation mapping and graph analysis of intrinsic connectivity in 144 healthy right-handers. *Brain Struct Funct* 224: 859–882, 2019. doi:10.1007/s00429-018-1810-2.
10. **Kong R**, **Li J**, **Orban C**, **Sabuncu MR**, **Liu H**, **Schaefer A**, **Sun N**, **Zuo XN**, **Holmes AJ**, **Eickhoff SB**, **Yeo BTT.** Spatial topography of individual-specific cortical networks predicts human cognition, personality, and emotion. *Cereb Cortex* 29: 2533–2551, 2019 [Erratum in *Cereb Cortex* 31: 3974, 2021]. doi:10.1093/cercor/bhy123.
11. **Rosenberg MD**, **Finn ES**, **Scheinost D**, **Papademetris X**, **Shen X**, **Constable RT**, **Chun MM.** A neuromarker of sustained attention from whole-brain functional connectivity. *Nat Neurosci* 19: 165–171, 2016. doi:10.1038/nn.4179.
12. **Shen X**, **Finn ES**, **Scheinost D**, **Rosenberg MD**, **Chun MM**, **Papademetris X**, **Constable RT.** Using connectome-based predictive modeling to predict individual behavior from brain connectivity. *Nat Protoc* 12: 506–518, 2017. doi:10.1038/nprot.2016.178.
13. **Buckholtz JW**, **Meyer-Lindenberg A.** Psychopathology and the human connectome: toward a transdiagnostic model of risk for mental illness. *Neuron* 74: 990–1004, 2012. doi:10.1016/j.neuron.2012.06.002.
14. **Gratton C**, **Koller JM**, **Shannon W**, **Greene DJ**, **Maiti B**, **Snyder AZ**, **Petersen SE**, **Perlmutter JS**, **Campbell MC.** Emergent functional network effects in Parkinson disease. *Cereb Cortex* 29: 2509–2523, 2019 [Erratum in *Cereb Cortex* 29: 1701, 2019]. doi:10.1093/cercor/bhy121.
15. **van den Heuvel MP**, **Sporns O**, **Collin G**, **Scheewe T**, **Mandl RC**, **Cahn W**, **Goñi J**, **Hulshoff Pol HE**, **Kahn RS.** Abnormal rich club organization and functional brain dynamics in schizophrenia. *JAMA Psychiatry* 70: 783–792, 2013. doi:10.1001/jamapsychiatry.2013.1328.
16. **Osher DE**, **Brissenden JA**, **Somers DC.** Predicting an individual's dorsal attention network activity from functional connectivity fingerprints. *J Neurophysiol* 122: 232–240, 2019. doi:10.1152/jn.00174.2019.

17. **Tavor I**, **Parker Jones O**, **Mars RB**, **Smith SM**, **Behrens TE**, **Jbabdi S.** Task-free MRI predicts individual differences in brain activity during task performance. *Science* 352: 216–220, 2016. doi:10.1126/science.aad8127.
18. **Tobyne SM**, **Somers DC**, **Brissenden JA**, **Michalka SW**, **Noyce AL**, **Osher DE.** Prediction of individualized task activation in sensory modality-selective frontal cortex with 'connectome fingerprinting'. *NeuroImage* 183: 173–185, 2018. doi:10.1016/j.neuroimage.2018.08.007.
19. **Kanwisher N.** Functional specificity in the human brain: a window into the functional architecture of the mind. *Proc Natl Acad Sci USA* 107: 11163–11170, 2010. doi:10.1073/pnas.1005062107.
20. **Drobyshevsky A**, **Baumann SB**, **Schneider W.** A rapid fMRI task battery for mapping of visual, motor, cognitive, and emotional function. *NeuroImage* 31: 732–744, 2006. doi:10.1016/j.neuroimage.2005.12.016.
21. **Madkhali Y**, **Aldehmi N**, **Pollick F.** Functional localizers for motor areas of the brain using fMRI. *Comput Intell Neurosci* 2022: 7589493, 2022. doi:10.1155/2022/7589493.
22. **Grill-Spector K**, **Weiner KS.** The functional architecture of the ventral temporal cortex and its role in categorization. *Nat Rev Neurosci* 15: 536–548, 2014. doi:10.1038/nrn3747.
23. **Julian JB**, **Fedorenko E**, **Webster J**, **Kanwisher N.** An algorithmic method for functionally defining regions of interest in the ventral visual pathway. *NeuroImage* 60: 2357–2364, 2012. doi:10.1016/j.neuroimage.2012.02.055.
24. **Kanwisher N**, **Dilks DD.** The functional organization of the ventral visual pathway in humans. In: *The New Visual Neurosciences*, edited by Chalupa L, Werner J. Cambridge, MA: MIT Press, 2013, p. 733–748.
25. **Weiner KS**, **Grill-Spector K.** Sparsely-distributed organization of face and limb activations in human ventral temporal cortex. *NeuroImage* 52: 1559–1573, 2010. doi:10.1016/j.neuroimage.2010.04.262.
26. **Fedorenko E**, **Hsieh PJ**, **Nieto-Castañón A**, **Whitfield-Gabrieli S**, **Kanwisher N.** New method for fMRI investigations of language: defining ROIs functionally in individual subjects. *J Neurophysiol* 104: 1177–1194, 2010. doi:10.1152/jn.00032.2010.
27. **Fedorenko E**, **Behr MK**, **Kanwisher N.** Functional specificity for high-level linguistic processing in the human brain. *Proc Natl Acad Sci USA* 108: 16428–16433, 2011. doi:10.1073/pnas.1112937108.
28. **Fedorenko E**, **Duncan J**, **Kanwisher N.** Language-selective and domain-general regions lie side by side within Broca's area. *Curr Biol* 22: 2059–2062, 2012. doi:10.1016/j.cub.2012.09.011.
29. **Fedorenko E**, **Thompson-Schill SL.** Reworking the language network. *Trends Cogn Sci* 18: 120–126, 2014. doi:10.1016/j.tics.2013.12.006.
30. **Kanwisher N**, **McDermott J**, **Chun MM.** The fusiform face area: a module in human extrastriate cortex specialized for face perception. *J Neurosci* 17: 4302–4311, 1997. doi:10.1523/JNEUROSCI.17-11-04302.1997.
31. **Frost MA**, **Goebel R.** Measuring structural-functional correspondence: spatial variability of specialised brain regions after macro-anatomical alignment. *NeuroImage* 59: 1369–1381, 2012. doi:10.1016/j.neuroimage.2011.08.035.
32. **Saxe R**, **Brett M**, **Kanwisher N.** Divide and conquer: a defense of functional localizers. *NeuroImage* 30: 1088–1096, 2006. doi:10.1016/j.neuroimage.2005.12.062.
33. **Dilks DD**, **Kamps FS**, **Persichetti AS.** Three cortical scene systems and their development. *Trends Cogn Sci* 26: 117–127, 2022. doi:10.1016/j.tics.2021.11.002.
34. **Vul E**, **Harris C**, **Winkielman P**, **Pashler H.** Puzzlingly high correlations in fMRI studies of emotion, personality, and social cognition. *Perspect Psychol Sci* 4: 274–290, 2009. doi:10.1111/j.1745-6924.2009.01125.x.
35. **Arslan S**, **Ktena SI**, **Makropoulos A**, **Robinson EC**, **Rueckert D**, **Parisot S.** Human brain mapping: a systematic comparison of parcellation methods for the human cerebral cortex. *NeuroImage* 170: 5–30, 2018. doi:10.1016/j.neuroimage.2017.04.014.
36. **Blumensath T**, **Jbabdi S**, **Glasser MF**, **Van Essen DC**, **Ugurbil K**, **Behrens TE**, **Smith SM.** Spatially constrained hierarchical parcellation of the brain with resting state fMRI. *NeuroImage* 76: 313–324, 2013. doi:10.1016/j.neuroimage.2013.03.024.
37. **Chong M**, **Bhushan C**, **Joshi AA**, **Choi S**, **Haldar JP**, **Shattuck DW**, **Spreng RN**, **Leahy RM.** Individual parcellation of resting fMRI with a group functional connectivity prior. *NeuroImage* 156: 87–100, 2017. doi:10.1016/j.neuroimage.2017.04.054.
38. **Gordon EM**, **Laumann TO**, **Adeyemo B**, **Gilmore AW**, **Nelson SM**, **Dosenbach NUF**, **Petersen SE.** Individual-specific features of brain systems identified with resting state functional correlations. *NeuroImage* 146: 918–939, 2017. doi:10.1016/j.neuroimage.2016.08.032.
39. **Braga RM**, **DiNicola LM**, **Becker HC**, **Buckner RL.** Situating the left-lateralized language network in the broader organization of multiple specialized large-scale distributed networks. *J Neurophysiol* 124: 1415–1448, 2020. doi:10.1152/jn.00753.2019.
40. **Van Essen DC**, **Ugurbil K**, **Auerbach E**, **Barch D**, **Behrens TE**, **Bucholz R**, **Chang A**, **Chen L**, **Corbetta M**, **Curtiss SW**, **Della Penna S**, **Feinberg D**, **Glasser MF**, **Harel N**, **Heath AC**, **Larson-Prior L**, **Marcus D**, **Michalareas G**, **Moeller S**, **Oostenveld R**, **Petersen SE**, **Prior F**, **Schlaggar BL**, **Smith SM**, **Snyder AZ**, **Xu J**, **Yacoub E**; **WU-Minn HCP Consortium.** The Human Connectome Project: a data acquisition perspective. *NeuroImage* 62: 2222–2231, 2012. doi:10.1016/j.neuroimage.2012.02.018.
41. **Barch DM**, **Burgess GC**, **Harms MP**, **Petersen SE**, **Schlaggar BL**, **Corbetta M**, **Glasser MF**, **Curtiss S**, **Dixit S**, **Feldt C**, **Nolan D**, **Bryant E**, **Hartley T**, **Footer O**, **Bjork JM**, **Poldrack R**, **Smith S**, **Johansen-Berg H**, **Snyder AZ**, **Van Essen DC**; **WU-Minn HCP Consortium.** Function in the human connectome: task-fMRI and individual differences in behavior. *NeuroImage* 80: 169–189, 2013. doi:10.1016/j.neuroimage.2013.05.033.
42. **Glasser MF**, **Sotiropoulos SN**, **Wilson JA**, **Coalson TS**, **Fischl B**, **Andersson JL**, **Xu J**, **Jbabdi S**, **Webster M**, **Polimeni JR**, **Van Essen DC**, **Jenkinson M**; **WU-Minn HCP Consortium.** The minimal preprocessing pipelines for the Human Connectome Project. *NeuroImage* 80: 105–124, 2013. doi:10.1016/j.neuroimage.2013.04.127.
43. **Salimi-Khorshidi G**, **Douaud G**, **Beckmann CF**, **Glasser MF**, **Griffanti L**, **Smith SM.** Automatic denoising of functional MRI data: combining independent component analysis and hierarchical fusion of classifiers. *NeuroImage* 90: 449–468, 2014. doi:10.1016/j.neuroimage.2013.11.046.
44. **Arthur D**, **Vassilvitskii S.** k-means++: the advantages of careful seeding. In: *Proceedings of the Eighteenth Annual ACM-SIAM Symposium on Discrete Algorithms*. Philadelphia, PA: Society for Industrial and Applied Mathematics, 2007, p. 1027–1035.
45. **Lloyd S.** Least squares quantization in PCM. *IEEE Trans Inform Theory* 28: 129–137, 1982. doi:10.1109/TIT.1982.1056489.
46. **Haralick RM**, **Sternberg SR**, **Zhuang X.** Image analysis using mathematical morphology. *IEEE Trans Pattern Anal Mach Intell* 9: 532–550, 1987. doi:10.1109/TPAMI.1987.4767941.
47. **Tzourio-Mazoyer N**, **Labache L**, **Zago L**, **Hesling I**, **Mazoyer B.** Neural support of manual preference revealed by BOLD variations during right and left finger-tapping in a sample of 287 healthy adults balanced for handedness. *Laterality* 26: 398–420, 2021. doi:10.1080/1357650X.2020.1862142.
48. **Rosenke M**, **van Hoof R**, **van den Hurk J**, **Grill-Spector K**, **Goebel R.** A probabilistic functional atlas of human occipito-temporal visual cortex. *Cereb Cortex* 31: 603–619, 2021. doi:10.1093/cercor/bhaa246.
49. **Holm S.** A simple sequentially rejective multiple test procedure. *Scand J Statist* 6: 65–70, 1979.
50. **Osher DE**, **Saxe RR**, **Koldewyn K**, **Gabrieli JD**, **Kanwisher N**, **Saygin ZM.** Structural connectivity fingerprints predict cortical selectivity for multiple visual categories across cortex. *Cereb Cortex* 26: 1668–1683, 2016. doi:10.1093/cercor/bhu303.
51. **Saygin ZM**, **Osher DE**, **Koldewyn K**, **Reynolds G**, **Gabrieli JD**, **Saxe RR.** Anatomical connectivity patterns predict face selectivity in the fusiform gyrus. *Nat Neurosci* 15: 321–327, 2011. doi:10.1038/nn.3001.
52. **Cole MW**, **Bassett DS**, **Power JD**, **Braver TS**, **Petersen SE.** Intrinsic and task-evoked network architectures of the human brain. *Neuron* 83: 238–251, 2014. doi:10.1016/j.neuron.2014.05.014.
53. **Fox CJ**, **Iaria G**, **Barton JJ.** Defining the face processing network: optimization of the functional localizer in fMRI. *Hum Brain Mapp* 30: 1637–1651, 2009. doi:10.1002/hbm.20630.
54. **Dadi K**, **Varoquaux G**, **Machlouzarides-Shalit A**, **Gorgolewski KJ**, **Wassermann D**, **Thirion B**, **Mensch A.** Fine-grain atlases of functional modes for fMRI analysis. *NeuroImage* 221: 117126, 2020. doi:10.1016/j.neuroimage.2020.117126.
55. **Bijsterbosch J**, **Harrison SJ**, **Jbabdi S**, **Woolrich M**, **Beckmann C**, **Smith S**, **Duff EP.** Challenges and future directions for representations of functional brain organization. *Nat Neurosci* 23: 1484–1495, 2020. doi:10.1038/s41593-020-00726-z.
56. **Akiki TJ**, **Abdallah CG.** Determining the hierarchical architecture of the human brain using subject-level clustering of functional networks. *Sci Rep* 9: 19290, 2019. doi:10.1038/s41598-019-55738-y.

57. **Hacker CD**, **Laumann TO**, **Szrama NP**, **Baldassarre A**, **Snyder AZ**, **Leuthardt EC**, **Corbetta M.** Resting state network estimation in individual subjects. *NeuroImage* 82: 616–633, 2013. doi:10.1016/j.neuroimage.2013.05.108.
58. **Wang D**, **Buckner RL**, **Fox MD**, **Holt DJ**, **Holmes AJ**, **Stoecklein S**, **Langs G**, **Pan R**, **Qian T**, **Li K**, **Baker JT**, **Stufflebeam SM**, **Wang K**, **Wang X**, **Hong B**, **Liu H.** Parcellating cortical functional networks in individuals. *Nat Neurosci* 18: 1853–1860, 2015. doi:10.1038/nn.4164.
59. **Wig GS**, **Laumann TO**, **Cohen AL**, **Power JD**, **Nelson SM**, **Glasser MF**, **Miezin FM**, **Snyder AZ**, **Schlaggar BL**, **Petersen SE.** Parcellating an individual subject's cortical and subcortical brain structures using snowball sampling of resting state correlations. *Cereb Cortex* 24: 2036–2054, 2014. doi:10.1093/cercor/bht056.
60. **Kong R**, **Yang Q**, **Gordon E**, **Xue A**, **Yan X**, **Orban C**, **Zuo XN**, **Spreng N**, **Ge T**, **Holmes A**, **Eickhoff S**, **Yeo BTT.** Individual-specific areal-level parcellations improve functional connectivity prediction of behavior. *Cereb Cortex* 31: 4477–4500, 2021. doi:10.1093/cercor/bhab101.
61. **Eriksson J**, **Vogel EK**, **Lansner A**, **Bergström F**, **Nyberg L.** Neurocognitive architecture of working memory. *Neuron* 88: 33–46, 2015. doi:10.1016/j.neuron.2015.09.020.
62. **Stark DE**, **Margulies DS**, **Shehzad ZE**, **Reiss P**, **Kelly AM**, **Uddin LQ**, **Gee DG**, **Roy AK**, **Banich MT**, **Castellanos FX**, **Milham MP.** Regional variation in interhemispheric coordination of intrinsic hemodynamic fluctuations. *J Neurosci* 28: 13754–13764, 2008. doi:10.1523/JNEUROSCI.4544-08.2008.
63. **Toro R**, **Fox PT**, **Paus T.** Functional coactivation map of the human brain. *Cereb Cortex* 18: 2553–2559, 2008. doi:10.1093/cercor/bhn014.
64. **Yan X**, **Kong R**, **Xue A**, **Yang Q**, **Orban C**, **An L**, **Holmes AJ**, **Qian X**, **Chen J**, **Zuo XN**, **Zhou JH**, **Fortier MV**, **Tan AP**, **Gluckman P**, **Chong YS**, **Meaney MJ**, **Bzdok D**, **Eickhoff SB**, **Yeo BTT.** Homotopic local-global parcellation of the human cerebral cortex from resting state functional connectivity. *NeuroImage* 273: 120010, 2023. doi:10.1016/j.neuroimage.2023.120010.
65. **Knecht S**, **Dräger B**, **Deppe M**, **Bobe L**, **Lohmann H**, **Flöel A**, **Ringelstein EB**, **Henningsen H.** Handedness and hemispheric language dominance in healthy humans. *Brain* 123: 2512–2518, 2000. doi:10.1093/brain/123.12.2512.
66. **Joliot M**, **Jobard G**, **Naveau M**, **Delcroix N**, **Petit L**, **Zago L**, **Crivello F**, **Mellet E**, **Mazoyer B**, **Tzourio-Mazoyer N.** AICHA: an atlas of intrinsic connectivity of homotopic areas. *J Neurosci Methods* 254: 46–59, 2015. doi:10.1016/j.jneumeth.2015.07.013.
67. **Glasser MF**, **Coalson TS**, **Robinson EC**, **Hacker CD**, **Harwell J**, **Yacoub E**, **Ugurbil K**, **Andersson J**, **Beckmann CF**, **Jenkinson M**, **Smith SM**, **Van Essen DC.** A multi-modal parcellation of human cerebral cortex. *Nature* 536: 171–178, 2016. doi:10.1038/nature18933.
68. **Dosenbach NU**, **Nardos B**, **Cohen AL**, **Fair DA**, **Power JD**, **Church JA**, **Nelson SM**, **Wig GS**, **Vogel AC**, **Lessov-Schlaggar CN**, **Barnes KA**, **Dubis JW**, **Feczko E**, **Coalson RS**, **Pruett JR Jr**, **Barch DM**, **Petersen SE**, **Schlaggar BL.** Prediction of individual brain maturity using fMRI. *Science* 329: 1358–1361, 2010 [Erratum in *Science* 330: 756, 2010]. doi:10.1126/science.1194144.
69. **Gilmore JH**, **Knickmeyer RC**, **Gao W.** Imaging structural and functional brain development in early childhood. *Nat Rev Neurosci* 19: 123–137, 2018. doi:10.1038/nrn.2018.1.
70. **Arichi T**, **Fagiolo G**, **Varela M**, **Melendez-Calderon A**, **Allievi A**, **Merchant N**, **Tusor N**, **Counsell SJ**, **Burdet E**, **Beckmann CF**, **Edwards AD.** Development of BOLD signal hemodynamic responses in the human brain. *NeuroImage* 63: 663–673, 2012. doi:10.1016/j.neuroimage.2012.06.054.
71. **Deen B**, **Richardson H**, **Dilks DD**, **Takahashi A**, **Keil B**, **Wald LL**, **Kanwisher N**, **Saxe R.** Organization of high-level visual cortex in human infants. *Nat Commun* 8: 13995, 2017. doi:10.1038/ncomms13995.
72. **Gomez J**, **Zhen Z**, **Weiner KS.** Human visual cortex is organized along two genetically opposed hierarchical gradients with unique developmental and evolutionary origins. *PLoS Biol* 17: e3000362, 2019. doi:10.1371/journal.pbio.3000362.
73. **Saygin ZM**, **Osher DE**, **Norton ES**, **Youssoufian DA**, **Beach SD**, **Feather J**, **Gaab N**, **Gabrieli JD**, **Kanwisher N.** Connectivity precedes function in the development of the visual word form area. *Nat Neurosci* 19: 1250–1255, 2016. doi:10.1038/nn.4354.
74. **van den Heuvel MP**, **Sporns O.** A cross-disorder connectome landscape of brain dysconnectivity. *Nat Rev Neurosci* 20: 435–446, 2019. doi:10.1038/s41583-019-0177-6.